

Contents lists available at ScienceDirect

Journal of Energy Chemistry

journal homepage: www.elsevier.com/locate/jechem



http://www.journals.elsevier.com/

Fabrication of multi-shell coated silicon nanoparticles via *in-situ* electroless deposition as high performance anodes for lithium ion batteries

Wen-Feng Ren^a, Jun-Tao Li^{b,*}, Shao-Jian Zhang^b, Ai-Ling Lin^b, You-Hu Chen^a, Zhen-Guang Gao^b, Yao Zhou^b, Li Deng^b, Ling Huang^a, Shi-Gang Sun^{a,b,**}

^a State Key Laboratory of Physical Chemistry of Solid Surfaces, iChEM (Collaborative Innovation Center of Chemistry for Energy Materials), College of Chemistry and Chemical Engineering, Xiamen University, Xiamen 361005, Fujian, China
^b College of Energy, Xiamen University, Xiamen 361005, Fujian, China

ARTICLE INFO

Article history: Received 7 November 2019 Revised 4 January 2020 Accepted 5 January 2020 Available online 10 January 2020

Keywords: Silicon nanoparticles Multi-shell coating Electroless deposition Anode materials Lithium ion batteries

ABSTRACT

Si-based materials have been extensively studied because of their high theoretical capacity, low working potential, and abundant reserves, but serious initial irreversible capacity loss and poor cyclic performance resulting from large volume change of Si during lithiation and delithiation processes restrict their widespread application. Herein, we report the preparation of multi-shell coated Si (DS-Si) nanocomposites by *in-situ* electroless deposition method using Si granules as the active materials and copper sulfate as Cu sources. The ratio of Si and Cu was readily tuned by varying the concentration of copper sulfate. The multi-shell (Cu@Cu_xSi/SiO₂) coating on Si surface promotes the formation of robust and dense SEI films and the transportation of electron. Thus, the obtained DS-Si composites exhibit an initial coulombic efficiency of 86.2%, a capacity of 1636 mAh g⁻¹ after 100 discharge–charge cycles at 840 mA g⁻¹, and an average charge capacity of 1493 mAh g⁻¹ at 4200 mA g⁻¹. This study provides a low-cost and large-scale approach to the preparation of nanostructured Si-metal composites anodes with good electrochemical performance for lithium ion batteries.

© 2020 Science Press and Dalian Institute of Chemical Physics, Chinese Academy of Sciences. Published by Elsevier B.V. and Science Press. All rights reserved.

1. Introduction

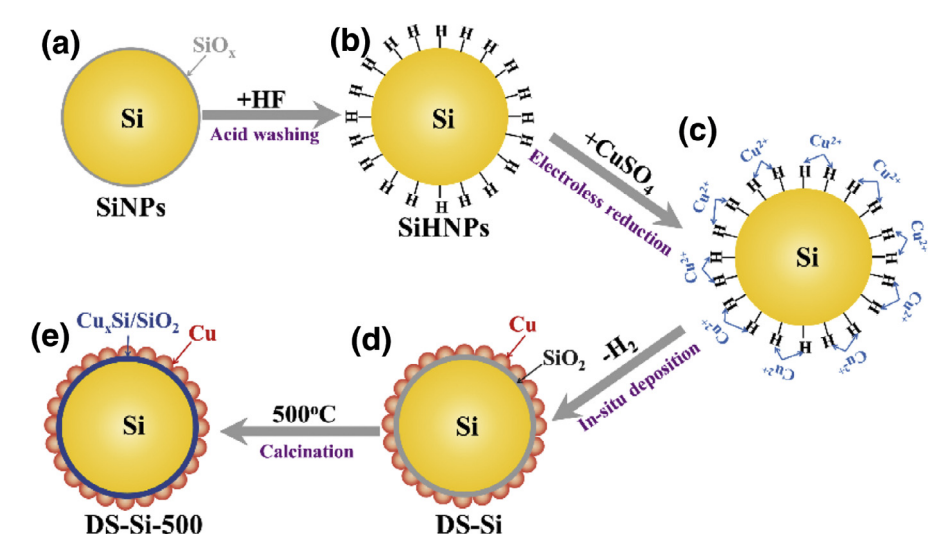
Developing high-energy lithium ion batteries is imperative to satisfy the demand in electric vehicles, energy storage, artificial intelligence, and 5G technology [1,2]. Among well-studied anode materials, Si is considered as a promising anode material resulting from its high theoretical specific capacity (4200 mAh g⁻¹, 10 times higher than graphite) and low working potential [3,4]. However, the large volume change (>300%) during Li–Si alloying and dealloying processes causes electrode cracks and pulverization and destroys SEI films on the surface of Si, resulting in the separation of Si with the current collector, the low coulombic efficiency, and the poor cyclability [5–7]. These disadvantages restrict the application of Si as lithium ion battery anodes.

E-mail addresses: jtli@xmu.edu.cn (J.-T. Li), sgsun@xmu.edu.cn (S.-G. Sun).

Many pioneering works demonstrated that the nanostructured core-shell Si/C composites are regarded as an effective method to solve the above challenges [8,9], in which nanostructured Si can hold the mechanical stress from volume change and carbon can facilitate electronic transmission and improve interface stability between electrode and electrolyte [10-13]. Nevertheless, the carbon coating layer suffers from its inherent stress limit and weak interaction with Si when the electrode is subjected to long-term cycling process [14]. The continuous volume change from the repeated Li-Si lithiation/delithiation processes eventually result in the crack of the coating layer and the separation of Si with conductive carbon, which leads to the continuous formation of excess SEI films, thus deteriorating ultimately the cycling performance. To address this issue, the metal coated layer with high conductivity and excellent ductility has been developed for improving both the conductivity and cyclability of Si-based electrodes [15-17]. For example, Yin et al. prepared nanostructured Si@Ag composites via directly mixing Si and Ag nanoparticles through ultrasonication in ethanol and drying processes, which exhibited stable electrode integrality and cycling performance compared with Si

^{*} Corresponding authors.

^{**} Corresponding author at: State Key Laboratory of Physical Chemistry of Solid Surfaces, iChEM (Collaborative Innovation Center of Chemistry for Energy Materials), College of Chemistry and Chemical Engineering, Xiamen University, Xiamen 361005, Fujian, China.



Scheme 1. The schematic diagram of the synthetic process of DS-Si composites.

Scheme 2. The formation process of hydrogen-passivation Si nanoparticles.

[18]. Cheng et al. reported core-shell Si@Ni nanocomposites within graphene nanosheets by oxidation-reduction reaction, graphene oxide reduction, and amino-modification methods, which could reach 2005 mAh g⁻¹ reversible capacity after 50 cycles [19]. Au et al. fabricated aligned Si@Cu nanorod arrays through oblique angle (co)deposition methods, exhibiting the capacity of 500 mAh g⁻¹ after 100 cycles for Si@Cu (3:7) composites [20]. Cetinkaya et al. produced core-shell Si@Cu composite powders using Si powders with 1-20 um diameters in size through sensitizing with SnCl₂ and HCl solution, then activating in a solution containing PdCl₂ and HCl, and coating with Cu derived from CuSO₄ solution using an electroless process [21]. The Si@Cu composite electrodes possessed the capacity retention with approximately 240 mAh g^{-1} after 20 cycles. Miroshnikov et al. confirmed that the metal coatedlayer could enhance the interconnectivity of the Si particles by almost 50% which increased the ratio of electroactive Si and enhanced the cyclability of Si-based anode materials [15]. However, the reported synthetic method possesses complex preparation processes and expensive instruments and raw materials. Importantly, the Si@metal composites prepared by physical mixing or chemical covering exist the weak interaction of Si with metal coated-layers, leading to the fall-off of the coated layer during the long-term cycling processes.

In this work, we developed an *in-situ* electroless deposition method for the preparation of multi-shell coated Si (DS-Si) nanocomposites where conductive multi-shell layer was homogeneously distributed on the surface and junction of Si nanoparticles bound by a Cu_xSi alloy through directly reacting Si nanoparticles with copper sulfate aqueous solution and heat treatment, which enables a good electrochemical performance owing to its superior electrical conductivity, the excellent metal ductility, the stable electrode/electrolyte interface, and the high utilization of Si. Furthermore, the ratios of Si and Cu were readily tuned by varying the concentration of copper sulfate. The as-synthesized coremulti shell structure promoted the formation of robust and dense SEI films and the transportation of electron on the surface of Si

nanoparticles, which exhibited improved initial coulomb efficiency, high reversible capacity, and good rate performance. This low-cost, simple and easy scale-up preparation method for DS-Si composite anodes with good electrochemical performance should contribute to the practical application of Si-based anodes in lithium ion batteries.

2. Experimental

2.1. Material synthesis

The multi-shell coated Si (DS-Si) nanocomposites were synthesized through an *in-situ* electroless deposition method. First, Si nanoparticles (SiNPs, average size of 50 nm, Alfa Aesar) were dispersed in hydrofluoric acid (5%) etching solution to eliminate surface oxidation layer of SiO_x and form hydrogen termination SiNPs (SiHNPs). After magnetic stirring for 15 min, the solution was filtrated and washed with de-ionized water. The obtained SiHNPs were dispersed in copper sulfate (CuSO₄·5H₂O, Sinopharm) solution with different concentrations (0.5, 1, 10, and 50 mmol L⁻¹) for 4 h. The resulting Cu@SiO₂-deposited Si (DS-Si) powders were filtered and washed with de-ionized water to remove the residual solution, and then dried in a vacuum oven at 100 °C for 10 h, denoted as DS-Si-1, DS-Si-2, DS-Si-3, and DS-Si-4. To increase the contact of Si and the coated layer, the obtained DS-Si-2 composites were sintered at 500 °C for 2 h, denoted as DS-Si-2-500.

2.2. Characterization

X-ray diffraction patterns (XRD) were carried out using a PANalytical X'Pert PRO MPD using the K_{α} radiation of Cu ($\lambda=1.5418$ Å). The microscopic features of the samples were observed using scanning electron microscopy (SEM, Hitachi S-4800) with energy dispersive X-ray (EDX) spectroscopy, transmission electron microscopy (TEM) and high-resolution TEM (HRTEM) (JEOL JEM-2100). Raman spectrum (XploRA, HORIBA) was recorded to collect the

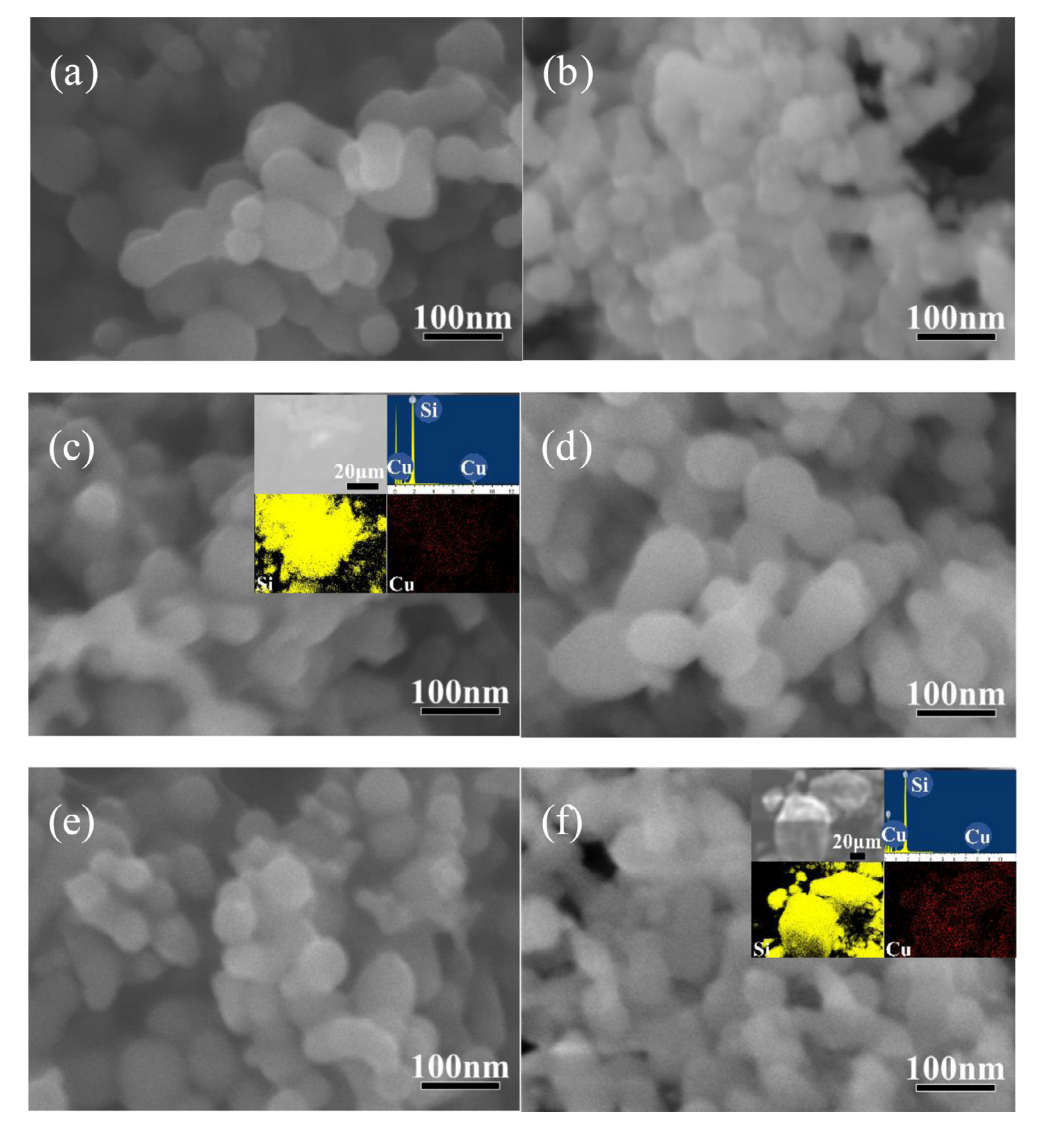


Fig. 1. SEM images of SiHNPs (a), DS-Si-1 (b), DS-Si-2 (c), DS-Si-3 (d), DS-Si-4 (e), and DS-Si-2-500 (f) (inserts are their EDX spectra and elemental mapping images).

detailed structure information. X-ray photoelectron spectroscopy (XPS) measurements were applied using PHI Quantum-2000 apparatus to analyze the surface elemental information.

2.3. Electrochemical measurement

The working electrodes were fabricated by mixing Si-based active materials, acetylene black conductive additives, and alginic acid sodium salt binder with a weight ratio of 50%:25%:25% with water as a solvent. The as-prepared slurries were cast onto the copper foil current collectors, dried at 40 °C for 24 h which was cut into 12 mm disks and then further dried at 100 °C in vacuum for 10 h. The mass loading of the active materials was around 0.7 mg cm⁻². CR2016 coin-type cells were assembled in an argon-filled glove box with polypropylene macroporous film (Celgard 2400) as the separator and lithium foil as the counter electrode. The liquid electrolyte consisted of LiPF₆ $(1 \text{ mol } L^{-1})$ in the mixture of ethylene carbonate, diethyl carbonate and dimethyl carbonate (with a volume ratio of 1:1:1) with the addition of vinylene carbonate (2 wt%) and fluoroethylene carbonate (10 wt%). The galvanostatic charge and discharge measurements were recorded by the Land battery test system (Wuhan, China) between 0.01 and 1.2 V at different current densities. Electrochemical impedance spectroscopy (EIS) tests were carried out using CHI660E electrochemical workstation with the frequency range from 100 kHz to 10 mHz at an ac-oscillation of 5 mV.

3. Results and discussion

The mechanism for the formation of the multi-shell coated Si (DS-Si) composites is depicted in Scheme 1, illustrating the pretreatment and deposition process. Firstly, Si nanoparticles (SiNPs) (Scheme 1a) were pretreated by hydrofluoric acid (HF) solution (5%) to eliminate surface oxidation layer of SiO_x and form surface hydrogen passivation layer. The Si-F bonds on the surface of SiNPs are formed during the reaction of SiO_x and HF, but the high electronegativity of F leads to the instability of Si-Si bonds. Thus, the Si atoms bonded with F atoms on the surface of SiNPs will be reacted with HF acid step by step, which produced the solid (SiH-NPs) and gas (SiF₄) residues. The formation mechanism of SiHNPs is shown in Scheme 2 [22,23]. SiHNPs (Scheme 1b) were collected after filtration and washing. After pretreatment, SiHNPs were dispersed in the solution of copper sulfate (CuSO₄) with different concentration. The Cu²⁺ ion were electroless reduced on the surface of SiHNPs and meanwhile generated H2 gas and Cu@SiO2 layer, as shown in Scheme 1(c) [24-26]. After filtration, washing and dry-

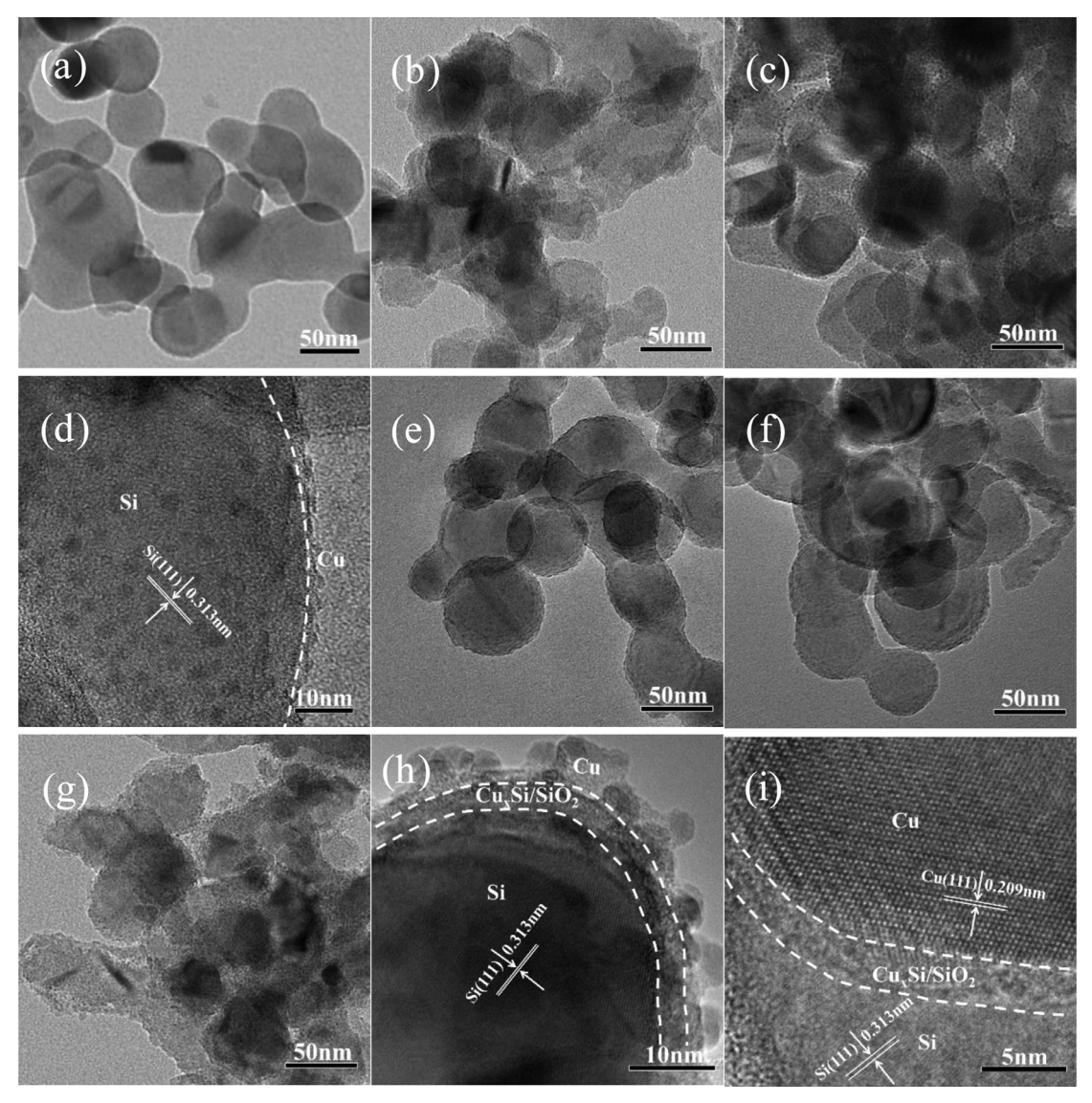


Fig. 2. TEM images of SiHNPs (a), DS-Si-1 (b), DS-Si-2 (c), DS-Si-3 (e), and DS-Si-4 (f), and (g) DS-Si-2-500; HRTEM images of DS-Si-2 (d) and DS-Si-2-500 (h and i).

ing, DS-Si composites (Scheme 1d) were obtained. To increase the contact of Si and Cu, the DS-Si-500 composites (Scheme 1e) were prepared after calcination of DS-Si composites at 500 °C and the Cu_xSi alloy were formed on the interface between Si and Cu, because the high reactivity between Si and Cu made Cu easy diffuse from SiO_2 -based dielectrics under thermal annealing to react with Si [27,28].

Fig. 1 presents the SEM images of SiHNPs and the obtained DS-Si composites. The SiHNPs present smooth surfaces and an average diameter of 50 nm, as shown in Fig. 1(a). One could see from Fig. 1(b-e) that as-synthesized DS-Si composites are assemblies of well-dispersed SiHNPs coated and bonded by Cu@SiO₂ gelatinoids. The EDX measurement reveals that the mass ratios of Cu in DS-Si composites are ~2.5% for DS-Si-1, ~3.4% for DS-Si-2, ~0.5% for DS-Si-3, and ~0.1% for DS-Si-4, indicating that the content of Cu decreases along with increasing the concentration of CuSO₄ solution, probably because the electrostatic repulsive force of Cu²⁺ would avoid the reduction of Cu²⁺ on the surface of pretreated SiHNPs. The highest content of Cu for DS-Si-2 indicates the optimal concentration of CuSO₄ benefits to the formation of Cu@SiO₂ layer on the surface and junction of Si. To improve the contact between Si and Cu, DS-Si composites were sintered at 500 °C. As sup-

ported in Fig. 1(f) for DS-Si-2-500, the gelatinoids layer disappears deriving from the improvement of crystallinity of Cu and the formation of Cu_xSi . The element mapping images (insert in Fig. 1(c) and (f)) of DS-Si-2 and DS-Si-2-500 reveal that the Si and Cu are uniform distributed in DS-Si composites. The well distributed and balanced $\text{Cu}_x\text{Cu}_x\text{Si}/\text{SiO}_2$ coated layer on the surface and junction of Si are expected to improve the electron transportation and the interface stability between the electrode and the electrolyte, maintain the electrode structural integrity, and increase the utilization of Si during the alloying and dealloying of Si, which would be further addressed in latter sections.

The TEM and HRTEM techniques were used to observe the formation of multi-coated layer on the surface and junction of SiH-NPs. Fig. 2(a) reveals that SiHNPs are smooth nanospheres with an average diameter of 50 nm. Shown by the TEM image of DS-Si composites in Fig. 2(b, c, e, and f), some Cu nanoparticles coated layer (about 3 nm) are anchored on the surface of SiHNPs after electroless deposition, which could help to improve electron transportation and electrode/electrolyte interface stability. Compared with DS-Si-1, DS-Si-3, and DS-Si-4, DS-Si-2 possesses the more Cu nanoparticles, consistent with the SEM and EDX results, indicating that the optimal concentration of CuSO₄ promotes the formation of

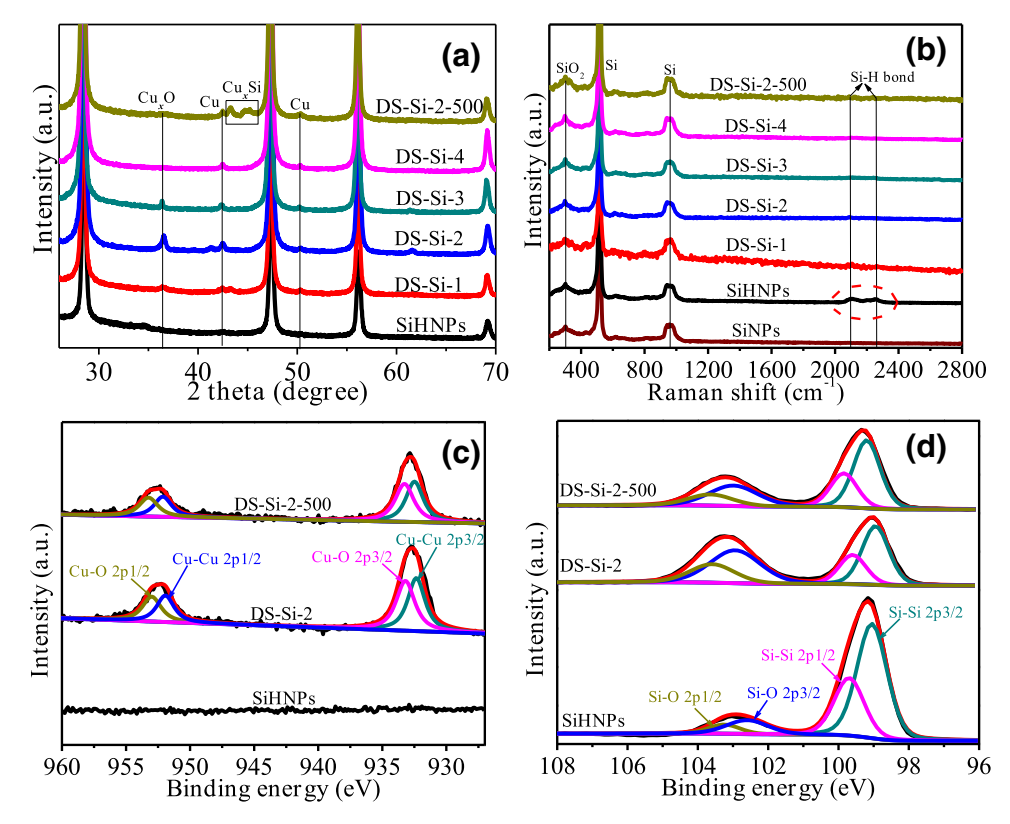


Fig. 3. XRD patterns (a), Raman spectra (b), and XPS spectra of Cu 2p (c) and Si 2p (d) of SiHNPs and DS-Si composites.

Cu nanoparticles. The HRTEM images of DS-Si-2 (Fig. 2(d)) clearly show the well resolved Si (111) lattice planes (0.313 nm) corresponding to the Si crystal and the well distributed Cu nanoparticles on the surface of SiHNPs. The Cu content is obviously less than that measured by EDX, due to the fall-off of Cu nanoparticles during the process of ultrasonic for the TEM measurement, indicating that the poor cohesiveness between Si and Cu. After calcination of DS-Si composites at 500 °C, for DS-Si-2-500 (Fig. 2(g)), more Cu particles are distributed on the surface and junction of Si compared with that of DS-Si-2, indicating that the process of calcination can avoid the fall-off of Cu granules and improve the contact between Si and Cu. The corresponding HRTEM image (Fig. 2(h) and (i)) further confirms the formation of the well distributed Cu granules layer (Cu(111), 0.209 nm) and Cu_xSi/SiO₂ interface layer on the surface of SiHNPs (Si(111), 0.313 nm). This core-multi shell DS-Si structure can enhance the electrochemical stability as it produces a stable electrode/electrolyte interface and increases the conductivity and mechanical property, which can efficiently withstand the volume change of Si during the repeated swelling and shrinking processes.

Fig. 3(a) shows the XRD patterns of SiHNPs and DS-Si composites. The distinct diffraction peaks of all the samples are corresponding to that of the crystal Si phase (JCPDS no. 27-1402) [29,30]. It is seen that the new reflection peaks at 2θ values of 42° and 50° were observed after coating, which corresponds to the FCC Cu crystal structure [21]. Besides, the Cu_xO phase at 2θ value of 37° may be formed during the electroless deposition period or be derived from the oxidation of Cu particles by air [31]. Compared with DS-Si-1, DS-Si-3, and DS-Si-4, DS-Si-2 exhibits stronger characteristic peaks for Cu and Cu_xO, consistent with SEM and TEM observation, indicating that the more Cu coated layer are formed using the optimal concentration of CuSO₄. After calcination at 500° C, the formation of Cu–Si alloy leads to the emerging of several weak diffraction peaks located at 43° – 45° , indicating the alloying reac-

tion with Si core derived from the Cu diffusion from SiO₂-based dielectrics under thermal annealing to react with Si [27,28,31,32]. The XRD patterns of DS-Si composites evidently confirm that the coated-layer is formed in the DS-Si composites, which can improve the conductivity and electrode/electrolyte interface stability of Si nanoparticles.

Fig. 3(b) presents the Raman spectra of SiNPs, SiHNPs, and DS-Si composites. Two peaks at ~517 and ~958 cm⁻¹ for all the samples confirm the existence of the crystalline Si [11]. Besides, for SiHNPs, Si-H local vibrational modes peaks at ~2111 and ~2257 cm⁻¹ can be seen obviously after HF acid treatment of SiNPs, which further confirm the above-mentioned mechanism [33,34]. After in-situ electroless deposition of Cu, the characteristic peaks of Si-H disappear and the peak intensity of SiO2 at ~300 cm⁻¹ increase, demonstrating the occurrence of the reaction between SiHNPs and CuSO₄. X-ray photoelectron spectroscopy (XPS) is measured to analyze the surface elemental composition and valence states of the SiHNPs and DS-Si composites. The narrow XPS spectra of Cu 2p are presented in Fig. 3(c). It is seen for DS-Si-2 and DS-Si-2-500 samples that there are the main peaks at ~933 eV and ~952 eV, corresponding to two asymmetric peaks of $2p_{3/2}$ and $2p_{1/2}$ for Cu-Cu and Cu-O, respectively, indicating the formation of Cu and Cu oxides on the surface of Si nanoparticles. However, for SiHNPs, there is no peak between ~925 eV and ~960 eV, suggesting the inexistence of Cu. The Si 2p spectra in Fig. 3(d) show that there are two main peaks at ~99 eV and ~103 eV consistent with Si-Si and Si-O peaks, respectively. The relative intensity of SiO₂:Si rise after in-situ electroless deposition and thermal treatment, signifying that the formation of more SiO₂ on Si surface for DS-Si composites, which further confirm the abovementioned mechanism.

Fig. 4(a) presents the 1st discharge/charge curves of SiHNPs and DS-Si composites at 420 mA g⁻¹ between 0.01 and 1.2 V. The lithiation voltage plateaus at 0.05–0.08 V in initial discharge curve and

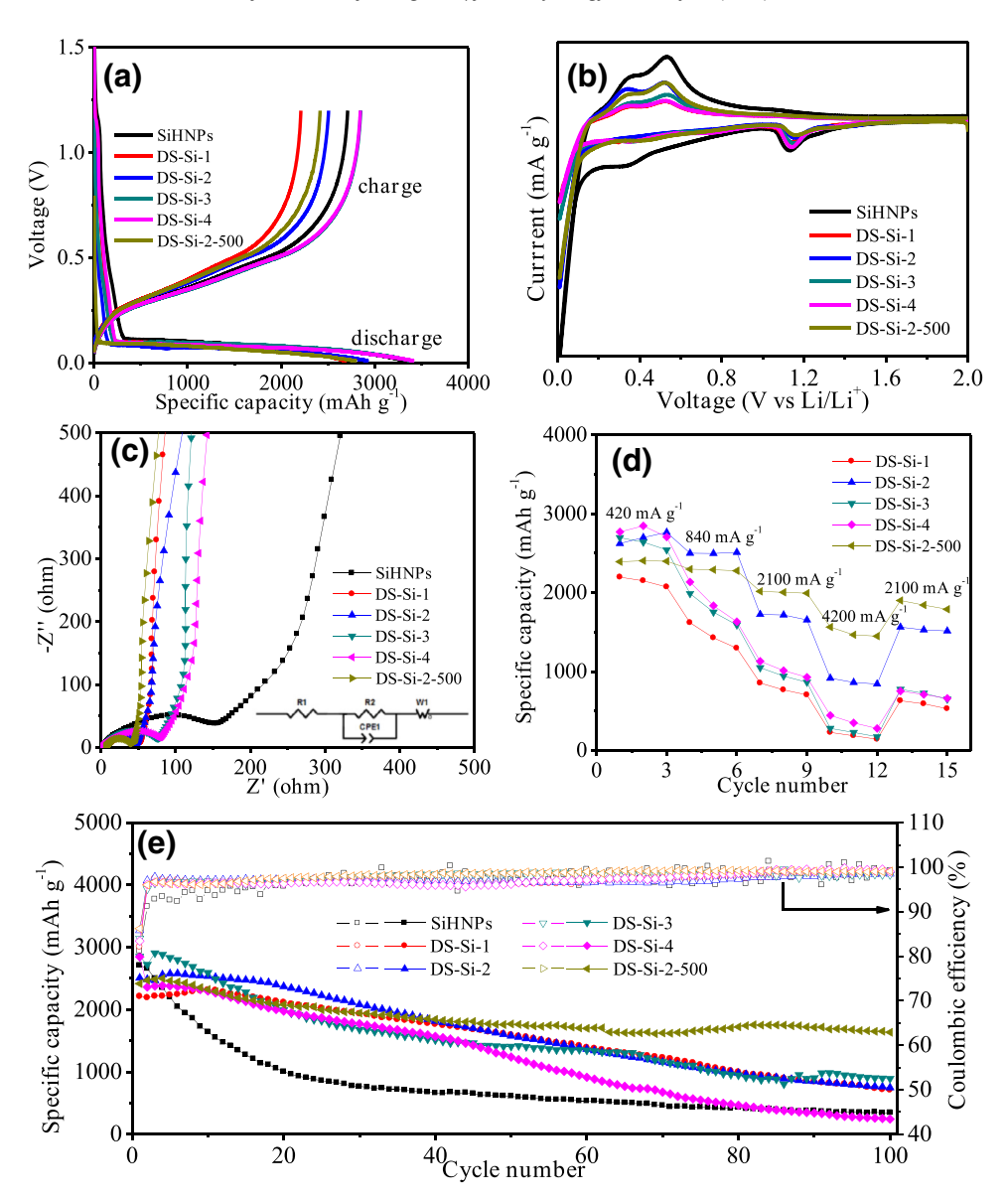


Fig. 4. Electrochemical performance of SiHNPs and DS-Si composite anodes: (a) the 1^{st} discharge/charge curves at 420 mA g^{-1} ; (b) CV curves for the 1^{st} cycle at a scan rate of 0.2 mV s^{-1} ; (c) electrochemical impedance spectra before cycling (insert is their equivalent circuits); (d) rate performance at different current densities, and (e) cycling performance and corresponding coulombic efficiency at 840 mA g^{-1} .

the delithiation voltage plateau at 0.25–0.65 V in initial charge curve are corresponding to the Si–Li alloying and dealloying processes, respectively [35]. The DS-Si-2 sample possesses high initial coulombic efficiency (85.7%), indicating that the optimal Cu@SiO_2 coated-layers can avoid the electrolyte decomposition clearly and form the stable SEI films [36]. Besides, the higher initial coulombic efficiency of DS-Si-2-500 (86.2%) than other DS-Si samples is associated with the formation of Cu_xSi alloy for improving the contact between Si nanoparticles and Cu coated-layer.

The cyclic voltammetry (CV) curves are measured between 0.01 V and 2.0 V with a scanning rate of 0.2 mV s $^{-1}$ for the 1st cycle, as shown in Fig. 4(b). During the first cathodic process, besides the peaks prominent at 0.16 V and 0.04 V related to the phase transition between Si and Li–Si alloys, there is an obvious peak at \sim 1.2 V corresponding the formation of SEI films resulting from the reduction of fluoroethylene carbonate in the electrolyte. The peak areas decrease after multi-shell coating on Si surface, indicating that the coated layer can avoid the formation of more SEI films. But for SiHNPs, the irreversible peak at 0.4–0.6 V related to

the decomposition of carbonate solvents in the electrolyte is also presented, probably because the swell of bare SiHNPs leads to the contact between fresh Si surface and the electrolyte to form more SEI films. The anodic peaks of all the samples appear at 0.30 and 0.51 V, which correspond to the phase transition from amorphous Li_xSi to amorphous Si.

Fig. 4(c) presents the electrochemical impedance spectra of Si-HNPs and DS-Si composites before cycling. The equivalent circuit is inserted in Fig. 4(c), which represents the electrochemical process roughly by a single R2 (charge transfer resistance) with CPE1 and Warburg element (W) for the diffusion of lithium ions. The semicircles (R2) of all samples are different in this order: SiHNPs (194 $\Omega)$ > DS-Si-4 (89 $\Omega)$ > DS-Si-3 (84 $\Omega)$ > DS-Si-1 (56 $\Omega)$ > DS-Si-2 (50 $\Omega)$ > DS-Si-2-500 (40 Ω). The diameters of the depressed semicircle of DS-Si composites are obviously less than that of SiHNPs, because the conductive multi-shell layer on the surface and junction of Si in the former one could increase the conductivity of electrode materials, as well as benefiting to the transportation of electrons. The resistance of DS-Si-2-500 is less than other

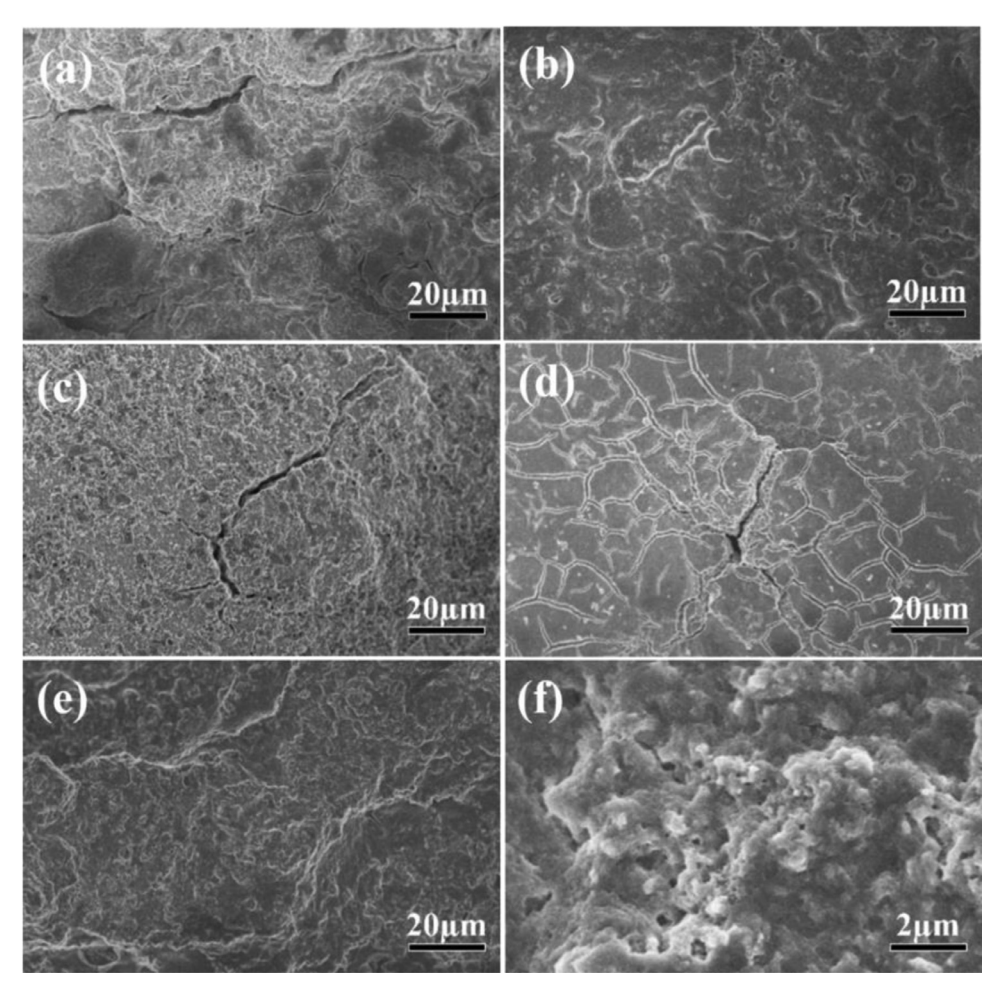


Fig. 5. SEM images of the cycled DS-Si-1 (a), DS-Si-2 (b), DS-Si-3 (c), DS-Si-4 (d), and DS-Si-2-500 (e and f) electrode disks after 100 discharge-charge cycles at 840 mA g⁻¹.

DS-Si composites, indicating the high-temperature calcination can increase the contact between Si and Cu through the formation of Cu_xSi which further facilitates the transportation of electrons.

The rate performance of DS-Si composites in Fig. 4(d) shows that the capacity of DS-Si-2 is higher than that of other DS-Si composites due to the conductive multi-shell layer on the surface and junction of Si promote the electronic transmission. At the higher current densities (2100 mA g^{-1} and 4200 mA g^{-1}), DS-Si-2-500 possesses the highest capacity, indicating that the hightemperature calcination can increase the contact between Si and Cu which further facilitates the improvement of rate performance. The cycling performance and corresponding coulombic efficiency of DS-Si composites measured at 840 mA $\rm g^{-1}$ between 0.01 and 1.2 V, as shown in Fig. 4(e). The better cycling performance of DS-Si composites than that of SiHNPs suggests that the Cu@SiO2 layers distributed on the surface and junction of Si promote the formation of stable electrode/electrolyte interface and maintain the electrode structural integrity during the alloying and dealloying of Si. After calcination at 500 °C, the improved cycling performance DS-Si-2-500 than other DS-Si samples is associated with the close contact between Si and Cu through the formation of Cu_xSi/SiO₂ interface layer.

Fig. 5 presents the surface SEM images of the cycled DS-Si composites electrode disks after 100 cycles at 840 mA $\rm g^{-1}$. Fig. 5(a, c and d) shows that there are obvious cracks and SEI films on the surface of the cycled DS-Si-1, DS-Si-3, and DS-Si-4 electrode disks. However, the cycled DS-Si-2 electrode disks (Fig. 5(b)) still maintains the structural integrity without cracks and possesses less SEI

films compared with other DS-Si composites, suggesting that the optimal of Cu@SiO₂ coated-layer contributes to maintain the electrode structure integrity and stabilize the interface between electrode and electrolyte. After calcination at 500 °C, it can be seen from Fig. 5(e and f) that there are clear porous structure with no cracks for the cycled DS-Si-2-500 electrode disks, which maintains the original surface morphology, indicating the strong contact between Si and Cu after the high-temperature calcination benefits to alleviate electrode deformation stress deriving from volume change during the repeated swelling/shrinking processes, which improves their electrochemical performance.

XPS spectra of SiHNPs and DS-Si composites after 1st cycle at 420 mA g⁻¹ were collected to investigate the influence of multi coated-layer on the formation of SEI films. The XPS spectra of C 1s (Fig. 6(a)) shows that the peak at ~290 eV is inexistent for DS-Si composites comparing with the bare SiHNPs, demonstrating that multi-shell coating can suppress the production of Li₂CO₃ and avoid the formation of excess SEI films on Si surface, which promotes the improvement of initial coulomb efficiency [37]. Fig. 6(b) presents the Cu 2p spectra of SiHNPs and DS-Si composites, indicating that there are two main peaks at ~932 eV and ~952 eV, corresponding to the $2p_{3/2}$ and $2p_{1/2}$ asymmetric peaks for Cu–Cu and Cu-O. The presence of Cu on cycled Si surface demonstrates that the SEI films cannot form on Cu surface, which assists electron transport to maintain the utilization of Si active materials. The weak peak of Si-Si and Si-O (Fig. 6(c)) for cycled DS-Si composites confirms the formation of robust and dense SEI films resulting from the multi-shell structure on Si surface [38]. Nevertheless,

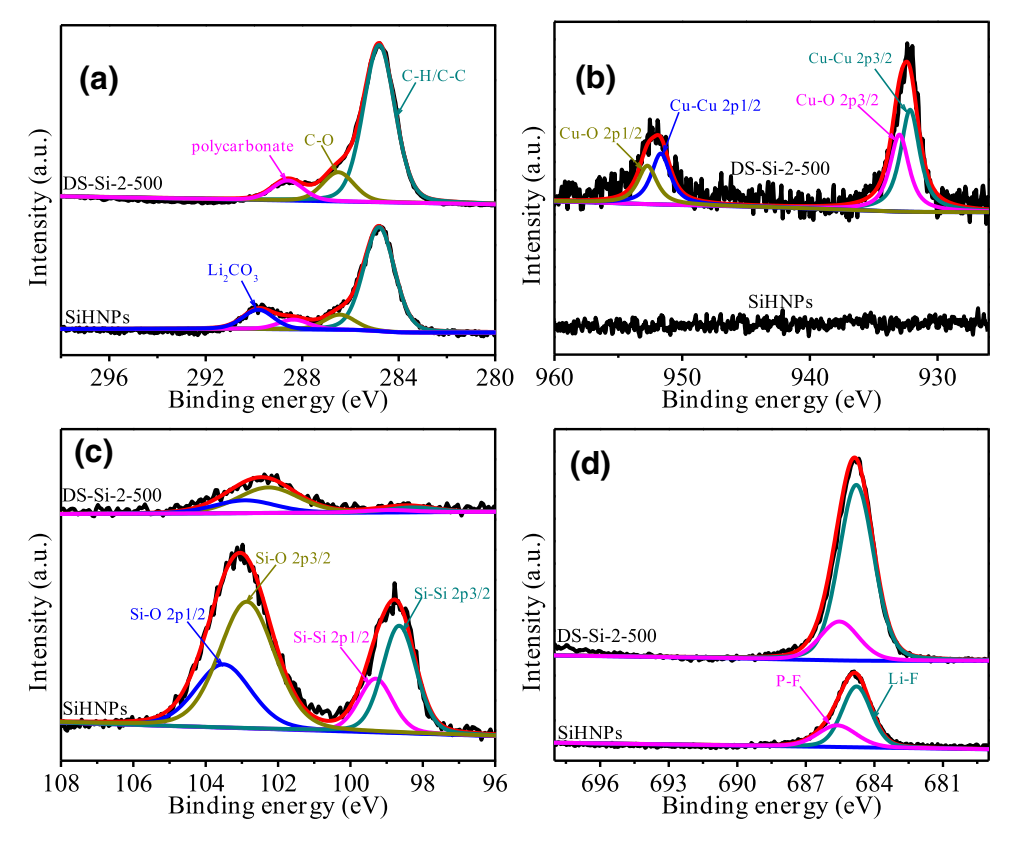
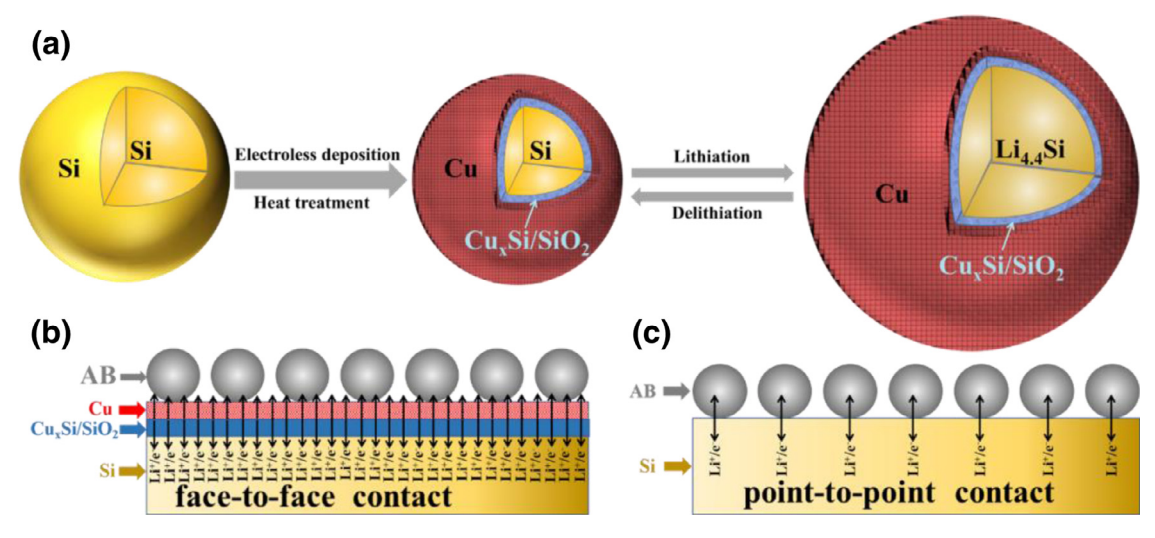


Fig. 6. XPS spectra of C 1s (a), Cu 2p (b), Si 2p (c), and F 1s (d) of SiHNPs and DS-Si composites after 1st cycle at 420 mA g⁻¹.



Scheme 3. The schematic visualization of electroless deposition and lithiation/delithiation processes of DS-Si composites (a) and the contact modes of DS-Si composites (b) and Si nanoparticles (c).

the obvious Si peaks for cycled SiHNPs after discharge–charge cycle indicate that the fresh Si surface exposes to the electrolyte to continuous form SEI films. The F 1s spectra demonstrate the more LiF for cycled DS-Si composites comparing with cycled SiHNPs, which promotes the production of stable SEI layers, as shown in Fig. 6(d) [39].

The obtained nanostructured DS-Si composites show high initial coulombic efficiency (86.2%), stable cycling performance (1636 mAh $\rm g^{-1}$ after 100 cycles) and good rate capability (1493 mAh $\rm g^{-1}$ at 4200 mA $\rm g^{-1}$), resulting from their special structure, as shown in Scheme 3. On the one hand, the well distributed

and balanced Cu@Cu_xSi/SiO₂ assemblies are formed on the surface and junction of Si by electroless deposition and heat treatment. Scheme 3(a) reveals that the core-multi shell DS-Si structure can promote the electrode/electrolyte interface stability and the maintenance of electrode integrity during the Si-Li alloying and dealloying processes. On the other hand, the presence of Cu@Cu_xSi/SiO₂ multi coated-layer on Si surface implements the face-to-face contact between Si and conductive coated-layer. Scheme 3(b) shows that the face-to-face contact structure induce the transportation of Li⁺ and e⁻ on all Si surface, comparing with the point-to-point contact (Scheme 3c) between Si nanoparticles and acetylene black

(AB) conductive additives. These advantages promote the enhancement of the overall electrochemical performance of Si-based anodes.

4. Conclusions

In summary, we have successfully fabricated nanostructured core-multi shell DS-Si composites by an in-situ electroless deposition method. The initial coulombic efficiency of DS-Si composites is 86.2%, higher than that of many reported Si-based anodes, indicating that Cu@CuxSi/SiO2 multi shell on Si surface can avoid the electrolyte decomposition obviously and form stable SEI films. DS-Si composite electrodes deliver a charge capacity of 1636 mAh g⁻¹ after 100 discharge-charge cycles at 840 mA $\rm g^{-1}$ and an average charge capacity of 1493 mAh g⁻¹ at 4200 mA g⁻¹, suggesting that the Cu@CuxSi/SiO2 multi shell distributed on the surface and junction of Si nanoparticles would benefits to the improvement of electrical conductivity, the electrode/electrolyte interface stability, the mechanical property, and the utilization of Si during the alloying and dealloying of Si. This low-cost, simple and easy scaleup preparation methods for the preparation of nanostructured Simetal composites with good electrochemical performance should promote the practical application of Si-based anodes in lithium ion batteries.

Declaration of Competing Interest

The authors declare that they have no known competing financial interests or personal relationships that could have appeared to influence the work reported in this paper.

Acknowledgments

This work was supported by the China Postdoctoral Science Foundation (2018M632575), the National Natural Science Foundation of China (21875197 and 21621091), and the National Key Research and Development of China (2016YFB0100202).

References

- J.W. Choi, D. Aurbach, Nat. Rev. Mat. 1 (2016) 16013, doi:10.1038/natrevmats. 2016.13.
- [2] J.Y. Li, Q. Xu, G. Li, Y.X. Yin, L.J. Wan, Y.G. Guo, Mater. Chem. Front. 1 (2017) 1691–1708, doi:10.1039/c6qm00302h.
- [3] K. Feng, M. Li, W. Liu, A.G. Kashkooli, X. Xiao, M. Cai, Z. Chen, Small 14 (2018) 1702737, doi:10.1002/smll.201702737.
- [4] W.F. Ren, Y. Zhou, J.T. Li, L. Huang, S.G. Sun, Curr. Opin. Electrochem. 18 (2019) 46–54, doi:10.1016/j.coelec.2019.09.006.
- [5] W. Luo, X. Chen, Y. Xia, M. Chen, L. Wang, Q. Wang, W. Li, J. Yang, Adv. Energy Mater. 7 (2017) 1701083, doi:10.1002/aenm.201701083.
 [6] X. Zuo, J. Zhu, P. Müller-Buschbaum, Y.J. Cheng, Nano Energy 31 (2017) 113-
- 143, doi:10.1016/j.nanoen.2016.11.013.
- [7] W. Ren, Y. Wang, Q. Tan, J. Yu, U.J. Etim, Z. Zhong, F. Su, Electrochim. Acta 320 (2019) 134625, doi:10.1016/j.electacta.2019.134625.
- [8] F. Luo, B. Liu, J. Zheng, G. Chu, K. Zhong, H. Li, X. Huang, L. Chen, J. Electrochem. Soc. 162 (2015) A2509–A2528, doi:10.1149/2.0131514jes.
- [9] L. Hu, B. Luo, C. Wu, P. Hu, L. Wang, H. Zhang, J. Energy Chem. 32 (2019) 124– 130, doi:10.1016/j.jechem.2018.07.008.

- [10] S. Chen, Z. Chen, X. Xu, C. Cao, M. Xia, Y. Luo, Small 14 (2018) 1703361, doi:10. 1002/smll.201703361.
- [11] W. Ren, Y. Wang, Q. Tan, Z. Zhong, F. Su, J. Power Sour. 332 (2016) 88–95, doi:10.1016/j.jpowsour.2016.09.110.
- [12] W. Ren, Z. Zhang, Y. Wang, Q. Tan, Z. Zhong, F. Su, J. Mater. Chem. A 3 (2015) 5859–5865, doi:10.1039/c4ta07093c.
- [13] W. Liu, J. Jiang, H. Wang, C. Deng, F. Wang, G. Peng, J. Energy Chem. 25 (2016) 817–824, doi:10.1016/j.jechem.2016.06.006.
- [14] G. Zheng, Y. Xiang, L. Xu, H. Luo, B. Wang, Y. Liu, X. Han, W. Zhao, S. Chen, H. Chen, Q. Zhang, T. Zhu, Y. Yang, Adv. Energy Mater. 8 (2018) 1801718, doi:10. 1002/aenm.201801718.
- [15] Y. Miroshnikov, J. Yang, V. Shokhen, M. Alesker, G. Gershinsky, A. Kraytsberg, Y. Ein-Eli, D. Zitoun, ACS Appl. Energy Mater. 1 (2018) 1096–1105, doi:10.1021/ acsaem.7b00220.
- [16] W. Yao, Y. Cui, L. Zhan, F. Chen, Y. Zhang, Y. Wang, Y. Song, Appl. Surf. Sci. 425 (2017) 614–621, doi:10.1016/j.apsusc.2017.06.031.
- [17] H. Li, M. Lu, W. Han, H. Li, Y. Wu, W. Zhang, J. Wang, B. Zhang, J. Energy Chem. 38 (2019) 50–54, doi:10.1016/j.jechem.2018.12.020.
- [18] S. Yin, Q. Ji, X. Zuo, S. Xie, K. Fang, Y. Xia, J. Li, B. Qiu, M. Wang, J. Ban, J. Mater. Sci. Technol. 34 (2018) 1902–1911, doi:10.1016/j.jmst.2018.02.004.
- [19] X.W. Cheng, D.L. Zhao, L.L. Wu, Z.W. Ding, T. Hu, S. Meng, Electrochim. Acta 265 (2018) 348–354, doi:10.1016/j.electacta.2018.01.198.
- [20] M. Au, Y. He, Y. Zhao, H. Ghassemi, R.S. Yassar, B. Garcia-Diaz, T. Adams, J. Power Sour. 196 (2011) 9640–9647, doi:10.1016/j.jpowsour.2011.07.022.
- [21] T. Cetinkaya, M. Uysal, M.O. Guler, H. Akbulut, A. Alp, Powder Technol. 253 (2014) 63–69, doi:10.1016/j.powtec.2013.11.004.
- [22] P. Thissen, E. Fuchs, K. Roodenko, T. Peixoto, B. Batchelor, D. Smith, W.G. Schmidt, Y. Chabal, J. Phys. Chem. C 119 (2015) 16947–16953, doi:10.1021/ acs.jpcc.5b03816.
- [23] T.C. Thi, K. Koyama, K. Ohdaira, H. Matsumura, Jpn. J. Appl. Phys. 55 (2016) 02BF09, doi:10.7567/JAP.55.02BF09.
- [24] T. Sham, I. Coulthard, J. Lorimer, A. Hiraya, M. Watanabe, Chem. Mater. 6 (1994) 2085–2091, doi:10.1021/cm00047a031.
- [25] X. Sun, H. Peng, Y. Tang, W. Shi, N. Wong, C. Lee, S. Lee, T. Sham, J. Appl. Phys. 89 (2001) 6396–6399, doi:10.1063/1.1367402.
- [26] I. Coulthard, T. Sham, Solid State Commun. 105 (1998) 751–754, doi:10.1016/ S0038-1098(97)10229-0.
- [27] J. Zhou, T. Gustafsson, E. Garfunkel, Surf. Sci. 372 (1997) 21–27, doi:10.1016/ S0039-6028(96)01100-4.
- [28] N. Benouattas, A. Mosser, D. Raiser, J. Faerber, A. Bouabellou, Appl. Surf. Sci. 153 (2000) 79–84, doi:10.1016/S0169-4332(99)00366-9.
- [29] T. Hatchard, J. Dahn, J. Electrochem. Soc. 151 (2004) A838–A842, doi:10.1149/ 1.1739217.
- [30] W. Ren, Y. Wang, Z. Zhang, Q. Tan, Z. Zhong, F. Su, J. Mater. Chem. A 4 (2016) 552–560, doi:10.1039/c5ta07487h.
- [31] J.H. Kim, H. Kim, H.J. Sohn, Electrochem. Commun. 7 (2005) 557–561, doi:10. 1016/j.elecom.2005.03.013.
- [32] H. Song, H.X. Wang, Z. Lin, X. Jiang, L. Yu, J. Xu, Z. Yu, X. Zhang, Y. Liu, P. He, L. Pan, Y. Shi, H. Zhou, K. Chen, Adv. Funct. Mater. 26 (2016) 524–531, doi:10. 1002/adfm.201504014.
- [33] J.F. Li, Y.F. Huang, Y. Ding, Z.L. Yang, S.B. Li, X.S. Zhou, F.R. Fan, W. Zhang, Z.Y. Zhou, D.Y. Wu, B. Ren, Z.L. Wang, Z.Q. Tian, Nature 464 (2010) 392–395, doi:10.1038/nature08907.
- [34] R. Saleh, N.H. Nickel, Thin Solid Films 427 (2003) 266–269, doi:10.1016/ s0040-6090(02)01203-8.
- [35] K. Ogata, S. Jeon, D.S. Ko, I.S. Jung, J.H. Kim, K. Ito, Y. Kubo, K. Takei, S. Saito, Y.H. Cho, H. Park, J. Jang, H.G. Kim, J.H. Kim, Y.S. Kim, W. Choi, M. Koh, K. Uosaki, S.G. Doo, Y. Hwang, S. Han, Nat. Commun. 9 (2018) 479, doi:10.1038/s41467-018-02824-w.
- [36] W.F. Ren, J.T. Li, Z.G. Huang, L. Deng, Y. Zhou, L. Huang, S.-.G. Sun, ChemElectroChem 5 (2018) 3258–3265, doi:10.1002/celc.201800834.
- [37] K. Yao, J.P. Zheng, R. Liang, J. Power Sour. 381 (2018) 164–170, doi:10.1016/j. jpowsour.2018.02.013.
- [38] Y.S. Hu, R. Demir-Cakan, M.M. Titirici, J.O. Müller, R. Schlögl, M. Antonietti, J. Maier, Angew. Chem. Int. Ed. 47 (2008) 1645–1649, doi:10.1002/anie. 200704287.
- [39] J. Zhao, Z. Lu, H. Wang, W. Liu, H.-.W. Lee, K. Yan, D. Zhuo, D. Lin, N. Liu, Y. Cui, J. Am. Chem. Soc. 137 (2015) 8372–8375, doi:10.1021/jacs.5b04526.